Society For Biomaterials

Experimental and numerical evaluation of drug release from nanofiber mats to brain tissue

Paweł Nakielski, Tomasz Kowalczyk, Krzysztof Zembrzycki, Tomasz A. Kowalewski

Institute of Fundamental Technological Research, Polish Academy of Sciences, 02-106 Warsaw, Poland

Received 23 January 2014; revised 31 March 2014; accepted 24 April 2014
Published online 00 Month 2014 in Wiley Online Library (wileyonlinelibrary.com). DOI: 10.1002/jbm.b.33197

Abstract: Drug delivery systems based on nanofibrous mats appear to be a promising healing practice for preventing brain neurodegeneration after surgery. One of the problems encountered during planning and constructing optimal delivery system based on nanofibrous mats is the estimation of parameters crucial for predicting drug release dynamics. This study describes our experimental setup allowing for spatial and temporary evaluation of drug release from nanofibrous polymers to obtain data necessary to validate appropriate numerical models. We applied laser light sheet method to illuminate released fluorescent drug analog and CCD camera for imaging selected cross-section of the investigated volume. Transparent hydrogel was used as a brain tissue phantom. The proposed setup allows for continuous observation of drug analog (fluorescent dye) diffusion for time span of several weeks. Images captured at selected time intervals were processed to determine concentration profiles and drug release kinetics. We used presented method to evaluate drug release from several polymers to validate numerical model used for optimizing nanofiber system for neuroprotective dressing. © 2014 Wiley Periodicals, Inc. J Biomed Mater Res Part B: Appl Biomater 00B:000–000, 2014.

Key Words: brain phantom, drug delivery, laser light sheet, computational modeling, nanofibers

How to cite this article: Nakielski P, Kowalczyk T, Zembrzycki K, Kowalewski TA. 2014. Experimental and numerical evaluation of drug release from nanofiber mats to brain tissue. J Biomed Mater Res Part B 2014:00B:000–000.

INTRODUCTION

Drug delivery systems based on polymeric nanofibers are broadly examined for wound healing, bone repair and nerve regeneration applications.[1–4] Long-term, effective, and controllable delivery of therapeutic agents to the brain after neurosurgery is of great interest in therapy of cancer and neurodegenerative diseases. Main advantage of nanofibrous mats in the context of regenerative medicine is their structural similarity to extracellular collagen matrix,[5–7] and possibility of employing them for drug delivery systems.[8–11] Material composition or fiber arrangement can be adjusted to modify release process. Engineering of the material with desired porosity and fiber morphology affects diffusion transport and therefore opens possibility for controlling dynamics of drug release from the material.[12] The most common method for evaluation of the drug release from implantable systems is dipping the material in serum substitute with exchange of supernatant with fresh medium after preselected time intervals.[13] Depending on hydrophobic or hydrophilic properties of released drug, the composition of the serum substitute is based on the chemistry of released drug. Usually the release of hydrophobic drugs is conducted in 0.5% wt water solution of sodium dodecyl sulfate (SDS) that contains micelles capable of absorbing drug molecules. Hydrophilic drugs are released to phosphate buffered saline (PBS) water solution, which provides a physiological pH. The aliquots collected after predetermined time intervals are analyzed to provide quantitative data of released drug (or its fluorescent analog). Results are summarized in form of cumulative mass release graphs used to compare drug release from materials of different structure, composition or morphology. The characterization includes determination of burst release, time of reaching release plateau and its values.

Observed diffusion of model drug molecules in convection enhanced drug delivery was used to accurately quantify its concentration by optical analysis of light absorption.[14,15] Hydrogel substituting brain parenchyma was used as a medium. Model drug - bromophenol blue, was infused with adequate flow rate through capillary catheter immersed in the hydrogel. The authors used various types of capillaries: single opening at one end or possessing multiple holes along the length of catheter. Volumetric distribution of the dye was measured. Information about dye concentration was compared with data of concentration collected from animal model and numerical simulations. O'Brien et al.[16] presented absorption based optical method of dye distribution assessment in tissue phantoms were drug delivery

Correspondence to: P. Nakielski (e-mail: pnakiel@ippt.pan.pl)
Contract grant sponsors: European Social Fund, Human Capital Operational Programme, and National Centre for Research and Development Project; contract grant number: NR13008110

from single stent strut was evaluated in hydrogel, replicating blood vessel wall.

Laser light sheet method proposed for this study has been commonly used in fluid mechanics for flow visualization, especially for particle image velocimetry (PIV). This method combined with the fluorescent technique allows for imaging full concentration fields of selected cross-section of the investigated system.[17] Collection of fluorescent light coming only from a thin illuminated sheet of the material volume allows to avoid complicated and inaccurate evaluation of the spatial effects present in the light absorption methods.[14]

Here, we describe our attempts to use the proposed experimental setup to evaluate the nanofibrous drug delivery system using polyvinyl alcohol (PVA) hydrogel crosslinked with borax. This material was selected to imitate diffusion properties of brain parenchyma. Specific hydrogel composition was selected to avoid light scattering on polymer chains present in the gel. The use of the optically transparent hydrogel was necessary to observe undisturbed fluorescence of drug simulants Rhodamine B and Bovine Serum Albumin conjugated with fluorescein isothiocyanate (BSA-FITC) released from nanofibers.[18] The Rhodamine B (molecule radius equal to $r_m = 0.9$ nm) was selected as an analogue of alpha-tocopherol ($r_m = 0.92$ nm). Similarly, BSA-FITC ($r_m = 4.6$ nm) was found to be analogue of nerve growth factor (NGF, $r_m = 2.6$ nm), that we applied in our *in vivo* experiments. Measured dye concentration fields provide data for proposed numerical model, which takes into account nanofibrous material composition and drug release kinetics. The advantages of proposed experimental method are: fast hydrogel preparation and relatively simple experimental system. By this way we optimize preparation of materials and determine time dependent concentration of the drug analogs as the function of the position from nanofibrous implant. The information found may be used in estimation of toxicity levels of targeted drug and effectiveness of therapy. Methodology described in this work we used to optimize neuroprotective materials used for prevention of neurodegeneration after neurosurgical procedures executed on an animal model (rat).[19,20] In that studies we found that nanofibrous material made of poly(L-lactide-*co*-caprolactone) (PLC) polymer influenced glial scar formation and caused less neurodegeneration comparing to control group with brain tissue left unprotected.

MATERIALS AND METHODS

Hydrogel preparation

Polyvinyl alcohol (PVA) hydrogel crosslinked with borax was prepared by dissolving 3.2 g of PVA ($M_w = 72{,}000$ Da, degree of hydrolysis <89%, POCh, Poland) in 60 mL of deionized water at 85°C. Dissolution was conducted on the hot plate and temperature of stirred solution was maintained below 90°C. After complete dissolution of the polymer, 7 mL of 0.1*M* solution of borax (POCh, Poland) was added and entire solution was vigorously agitated for next 15 min. Hot hydrogel was pour to self made polycarbonate cuvette of dimension of 5 × 4 × 3 cm. Air bubbles present in the hydrogel were removed by placing hot hydrogel in a desiccator at reduced pressure. Once the hydrogel cooled, cuvette was protected from drying with Parafilm® and placed in 4°C for 24 h. Such prepared gel, after adjustment to room temperature, retained its mechanical properties and showed no flow after cuvette rotation. The gel is also transparent for the green laser light used for the fluorescence excitation.

Nanofibrous mats preparation

Materials. Poly(L-lactide-*co*-caprolactone) (PLC, Purasorb 7015 containing 70% L-lactide and 30% caprolactone units, specific density 1170 kg/m^3), poly(D,L-lactide-*co*-glycolide) (PDLG, Purasorb 5010 containing 50% D,L-lactide and 50% glycolide units) both supplied by Corbion-Purac, Biochem BV, Nederlands; chloroform ($CHCl_3$, POCh, Poland), *N*,*N*-dimethylformamide (DMF, POCh, Poland), Rhodamine B (Sigma Aldrich), bovine serum albumin conjugated with fluoresceine (BSA-FITC, Sigma Aldrich) and SPAN80 (Sigma Aldrich) were used without further purification. The electrospinning stock solution was prepared by dissolving 1 g of PLC polymer in 10 g of mixture of DMF and $CHCl_3$ 1:9 (wt/wt). Model drugs: Rhodamine B ($M_w = 479$ Da, excitation/emission 540/625 nm, diffusion coefficient in hydrogel $D_{0\text{-}RB} = 6.3 \times 10^{-11}$ m^2/s) and BSA-FITC ($M_w = 66$ kDa, excitation/emission 490/525 nm, diffusion coefficient in hydrogel $D_{0\text{-}BF} = 1.1 \times 10^{-11}$ m^2/s) were used.

Preparation of nanofibers with lipophilic Rhodamine B was as following: 2.5 mg or 4 mg of Rhodamine B was mixed with 1 g of polymer stock solution to obtain 2.8% and 4.4% wt of dye respectively, regarding to polymer mass. BSA-FITC nanofibers were prepared as following: 4 mg of hydrophilic BSA-FITC was first dissolved in 50 mg of deionized water and then added drop-wise to 1.3 g of polymer stock solution mixed with 20 mg of SPAN80. Solutions were vortexed for 30 minutes to prepare stable water in oil emulsion.

During electrospinning of polymer or emulsion solution flow rate was fixed at 800 μL/h, positive electric potential of the 1 kV/cm was applied to the blunt needle (26 G) serving as nozzle and spinning distance was set to 15 cm. Randomly oriented polymer nanofibers were collected on a rotating drum (2000 rpm) of the diameter of 1.5 cm covered with grounded aluminum foil. Prepared nanofibrous mat remained on the drum for subsequent 24 h to avoid the shrinkage of the material. Disks of the diameter of 5 mm cut from mat by paper puncher were ready for characterization and drug release evaluation.

Nanofibrous mats characterization

The morphology of the material was examined by Scanning Electron Microscopy (SEM, Jeol, JSM 6390 LV, Japan). Before the SEM imaging specimens of fibermats were sputtered with a gold (mini sputter coater Polaron, SC 7620, UK). Porosity of material was calculated by dividing the density of nanofibrous mat by PLC density (1.17 g/cm^3) according to method presented by Lee and Yang[21] and estimated to be about 50% (Table II).

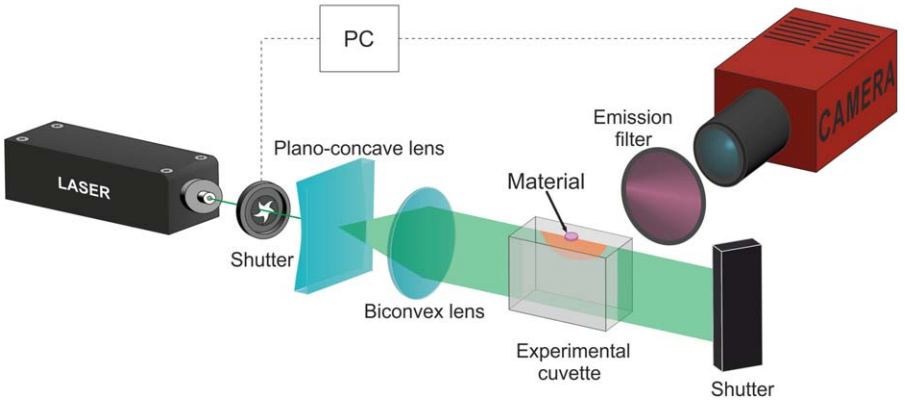

FIGURE 1. Experimental setup for drug release evaluation. From left to right: laser with excitation wavelength suitable for examined model drug, round shutter connected with PC, light sheet setup, nanofibrous material in experimental cuvette, emission filter suitable to pass wavelength corresponding to emission of examined model drug, camera connected with PC. [Color figure can be viewed in the online issue, which is available at wileyonlinelibrary.com.]

Drug release

Samples for release study were evaluated at 37°C in PBS buffer. Nanofibrous mat of approximately 1 cm^2 containing Rhodamine B or BSA-FITC was weighted to determine drug content and immersed in 1 mL water solution of 0.01*M* PBS. Supernatant fluid was exchanged with fresh medium at predetermined time intervals. Collected fluids were frozen until the end of experiment when the drug concentration was determined. Samples of 300 μL of collected supernatant were placed in 96-well microplate and fluorescence of Rhodamine B or BSA-FITC was read with fluorometer (Fluoroskan Ascent™ Microplate Fluorometer, Thermo Scientific, USA). Concentration of dyes was calculated with the use of calibration curve.

Experimental setup

A diagram of the experimental setup is presented in Figure 1. Laser beam of the wavelength 532 nm (for Rhodamine B determination) or 472 nm (for BSA-FITC determination) passes through the mechanical shutter connected to computer. Laser beam is converged to laser sheet by two lenses: plano-concave and biconvex (to collimate the light). The light sheet beam was then transmitted through cuvette filled with the hydrogel. The material was placed at the top of the gel. The emitted light passed through emission filter (602 ± 15 nm for Rhodamine B excitation and 540 ± 12 nm for BSA-FITC excitation respectively), and was recorded by a digital camera (Manta G-201B, Allied Vision Technologies, Germany). The camera was mounted on optical rail and raw images were recorded in tiff format. Camera settings were as following: exposure 400 ms, 5 fold amplification of the signal, constant white balance. To avoid photo bleaching of the measured fluorescent dye and to maintain laser stability, the light source was left in the ON position for duration of experiment and laser beam was stopped by the mechanical shutter connected to the computer. Opening of the shutter was coupled with image trigger and was controlled by the computer program written in MATLAB®.[22] A small amount of the light (approximately 5%) was reflected to photodiode (not shown in figure in order to simplify the scheme) to monitor intensity of laser light. The laser intensity was recorded during the whole experiment and used to normalize recorded fluorescence data. The release experiment was left unattended for several days or even weeks. During the whole acquisition period the images of the media fluorescence and the excitation laser intensity were automatically recorded every 5 min on the computer hard disk. The cuvette, emission filter and camera were covered from other sources of light to reduce the amount of ambient light interference.

The images captured during experiment were cropped manually to the size of interest. Values of pixel intensity at 0.5 mm from the center of the material (point P_1 in Figure 3) were collected for further processing. In most cases material did not relocate during experiment, the largest horizontal displacement of the material, measured after 4 days was 1 mm.

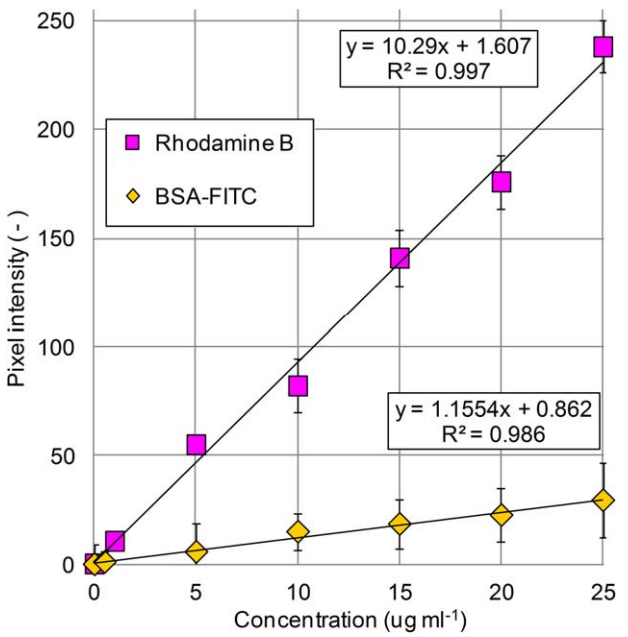

FIGURE 2. Calibration curves of Rhodamine B and BSA-FITC in PVA hydrogel. [Color figure can be viewed in the online issue, which is available at wileyonlinelibrary.com.]

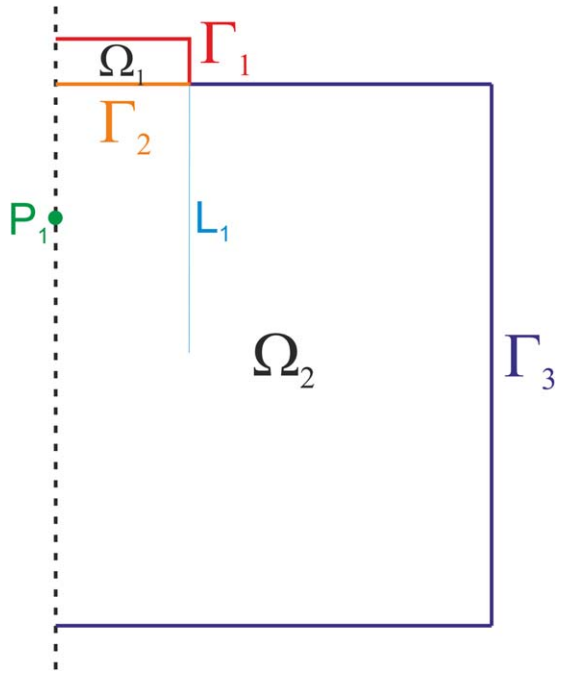

FIGURE 3. Domain and boundary representation in numerical model. Ω_1, Ω_2—represent material and PVA hydrogel domain respectively. The proportions of domains were not respected in this figure. The dotted line is axis symmetry of the domains. Γ_1, Γ_3—represent isolation boundary conditions and Γ_2 contact surface of the hydrogel and the material. P_1—point at which concentration value was compared with experimental data. L_1—line at which concentration value was presented in function of distance from the material. [Color figure can be viewed in the online issue, which is available at wileyonlinelibrary.com.]

In order to obtain quantitative information about released drug, calibration with known concentrations of model drugs in PVA hydrogel was performed. Calibration curves of Rhodamine B and BSA-FITC in PVA hydrogel are presented in Figure 2. Obtained value of pixel intensity for applied laser intensity and camera settings were close to maximum value of 255 for 8-bit camera. Attempts were done to obtain correct parameters of the camera in order to avoid saturation effect of pixels intensity. Calculated concentration of dyes in point P_1 (Figure 3) in the function of time (Figure 7) were used as an input for optimization of model parameters presented in section 3.

NUMERICAL MODEL OF DRUG RELEASE FROM NANOFIBROUS MATERIAL

Multi dimensional finite element analysis was adopted for complex geometries like convex tablets[23,24] and bulk degrading matrices[25] as a predictive tool to study drug release. Here, two dimensional finite element numerical model was used to solve in COMSOL Multiphysics® equations describing the drug release kinetics.[26] Concentration data collected from the experiments were used for model validation and subsequent material optimization. Initially model was developed for 3D concentration estimation in representative unit cell of material to find impact of fiber arrangement on drug delivery.[27] The transient adsorption - desorption process described by Langmuir isotherm was applied in the Ω_1 domain (Figure 3). Langmuir isotherm consider bimolecular reaction between model drug molecule C_B and unoccupied site ($C_A^{max} - C_A$), where C_A^{max} is maximum concentration of adsorbed drug on the material surface.

Model is based on the diffusion effective coefficients and sorption process. Material porosity is calculated comparing average specific density of the material and that of the polymer:

$$\varepsilon = 1 - \frac{\rho_m}{\rho_p} \tag{1}$$

where ρ_m is average material density (kg/m^3), and ρ_p is polymer density (kg/m^3).

Basic assumptions of the model employing Langmuir isotherm are:

- mono-layer drug coverage on the fiber surface,
- equivalence of every empty adsorption site,
- no polymer degradation effects,
- homogenous distribution of drug at the beginning of the release process,
- initial concentration of drug in PVA hydrogel Ω_2 domain is equal zero,
- diffusion of the drug in the PVA hydrogel is described by Fick's law.

The change of adsorbed drug concentration in nanofibrous material (Ω_1 domain) is expressed by Langmuir isotherm with adsorption–desorption terms:

$$\frac{dC_A}{dt} = k_{ads}\left(C_A^{max} - C_A\right)C_B - k_{des}\,C_A \tag{2}$$

where C_A is drug concentration adsorbed on the surface, expressed in relation to the weight of the polymer material (kg/kg), C_B is concentration of desorbed drug in hydrogel filling pores of nanofibrous mat (kg/m^3), k_{ads}, k_{des}—adsorption (m^3/kg·s), desorption (1/s) constant rates respectively.

TABLE I. Characteristics of the Materials

Mat nr	Dye	Concentration of Dye (%)	Polymer	Fiber Diameter (μm)	Porosity (%)	D_{Beff}/D_0	D_{Beff} (m^2/s)
M1	RB	2.8	PDLG	1.97 ± 0.85	55	0.38	$2.4\cdot\times 10^{-11}$
M2	RB	4.4	PDLG	1.92 ± 0.61	50	0.32	$2.0\cdot\times 10^{-11}$
M3	BF	2	PDLG	4.86 ± 0.30	40	0.21	$2.4\cdot\times 10^{-12}$
M4	BF	2	PLC	3.68 ± 0.25	40	0.20	$2.3\cdot\times 10^{-12}$

RB: Rhodamine B, BF: BSA-FITC.

TABLE II. Kinetic Parameters Calculated for Materials Analyzed in PVA Hydrogel and PBS

		k_{des} (m^3/kg·s)		k_{ads} (1/s)		k_c (m/s)	
Mat nr	Dye	PVA (10^{-4})	PBS (10^{-5})	PVA (10^{-6})	PBS (10^{-5})	PVA (10^{-7})	PBS (10^{-10})
M1	RB	1.4	0.52	6.7	0.44	1.4	32
M2	RB	0.76	1.0	0.01	0.35	0.1	35
M3	BF	2.5	1.2	2.5	1.1	2.2	0.27
M4	BF	3.1	5.6	24	6.5	2.3	0.24

RB: Rhodamine B, BF: BSA-FITC.

The spatiotemporal variation of drug concentration in Ω_1 domain (Figure 3) is described by diffusion term with effective diffusion coefficient D_{Beff} and sorption kinetics:

$$\frac{\partial C_B}{\partial t} = D_{B\ \mathrm{eff}}\left(\frac{\partial^2 C_B}{\partial x^2} + \frac{\partial^2 C_B}{\partial y^2}\right) - \frac{1-\varepsilon}{\varepsilon}\rho_p \frac{dC_A}{dt} \tag{3}$$

where x, y are spatial coordinates (m), ε is the porosity of the mat (−), ρ_p is polymer density (kg/m^3).

Flux balance boundary condition was applied on Γ_2 boundary (Figure 3) representing contact surface of the material and hydrogel:

$$N_B = N_C = k_c\left(C_B^{\mathrm{surf}} - C_B\right) = k_c\left(C_C^{\mathrm{surf}} - C_C\right) \tag{4}$$

where N_B, N_C are drug flux through the boundary; C_B^{surf}, C_C^{surf} are drug concentrations at the contact surface Γ_2; C_B, C_C are drug concentrations in PVA hydrogel (Ω_1, Ω_2 domain respectively). The mass transfer coefficient k_c (m/s) express mass transport resistance through the boundary Γ_2. Low value of k_c cause significant decrease in mass flux and drug retention in pores of the material as the step controlling the rate of the entire process.

On the remaining boundaries Γ_1, Γ_3 (Figure 3)—Neumann boundary conditions were applied which corresponds to isolation condition in the normal direction to the boundary $\vec{n}$.

$$D_{B\ \mathrm{eff}}\ \nabla c_A \cdot \vec{n} = 0 \tag{5}$$

The spatiotemporal variation of drug concentration in Ω_2 domain is described by diffusion transport of the model drug:

$$\frac{\partial C_C}{\partial t} = D_C\left(\frac{\partial^2 C_C}{\partial x^2} + \frac{\partial^2 C_C}{\partial y^2}\right) \tag{6}$$

where D_C is diffusion coefficient of dye in PVA hydrogel.

Initial drug concentrations in the Ω_1 domain: $C_A = C_A^{max} = C_{A0}$ (kg/kg) for the polymer material, and $C_{B0} = 0$ (kg/m^3) for the hydrogel. In Ω_2 domain $C_{C0} = 0$ (kg/m^3). Assumption of $C_A^{max} = C_{A0}$ (kg/kg) as an initial condition was dictated by the lack of suitable methods to find value of maximum concentration of the model drug on the surface of the nanofiber. After the material is placed on the top of the hydrogel, release process starts and continues until equilibrium is reached.

Diffusion coefficient of the drug in fluid is assumed to be constant. This coefficient is calculated from semi-empirical Eq. (7) which includes information about porosity of nanofibrous material, ratio of drug molecule to fiber diameter. For the calculation of diffusion coefficient we used equation proposed by Clague and Phillips,[28] which takes into account hydrodynamic and steric effects:

$$\frac{D_{B\ eff}}{D_0} = \mathrm{F} \cdot \mathrm{S} = \mathrm{e}^{-\mathrm{a}(1-\varepsilon)^{\mathrm{b}}} \cdot \mathrm{e}^{-0.84\mathrm{f}^{1.09}} \tag{7}$$

where D_{Beff}/D_0 express the ratio of diffusion coefficients in hydrogel with and without presence of the fibers, ε is the porosity of the material, $\mathrm{f} = (1-\varepsilon)(1+\lambda)^2$ is the corrected volume fraction expressed by λ. λ is the ratio of model drug molecule radius r_m (calculated from Einstein–Smoluchowski equation) to average fiber diameter r. Coefficient a and b were specified by Amsden[29] and are: $a = \pi$, $b = 0.174\ \ln\left(\frac{59.6}{\lambda}\right)$.

In order to find kinetic parameters of dye release from material immersed in fluid, discussed release model was

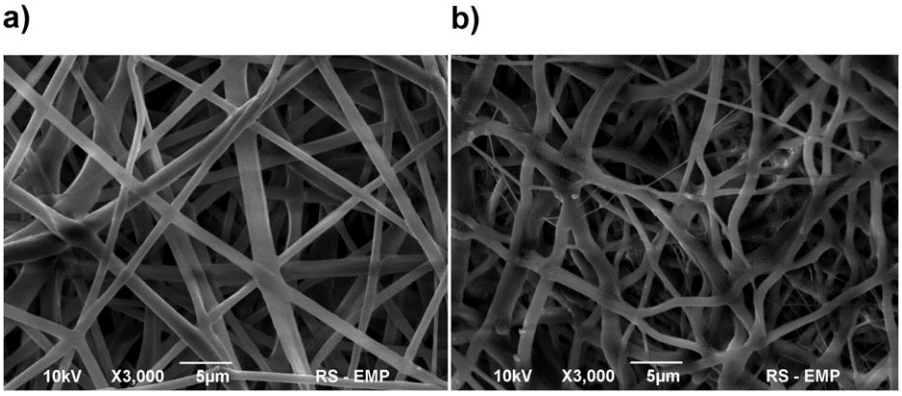

FIGURE 4. Comparison of SEM micrographs of two materials made from two polymers by emulsion electrospinning: a) PDLG polymer—M3, b) PLC polymer—M4.

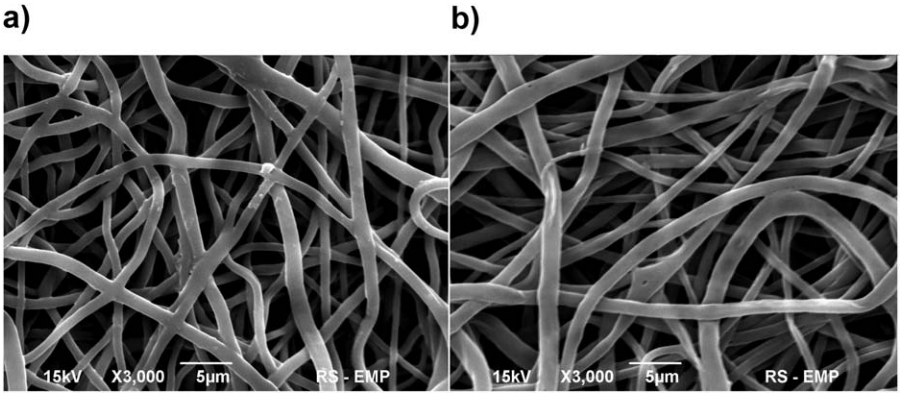

FIGURE 5. Morphology examination from SEM micrographs of two materials removed from the hydrogel after 4 days of drug release experiment. SEM micrographs present materials made from two polymers: a) PDLG polymer—M3, b) PLC polymer—M4.

modified to account only for Ω_1 material domain (Figure 3), from which dye was released to an infinite medium (perfect sink conditions). Additionally, boundary condition on Γ_1 and Γ_2 boundaries (Figure 3) were changed to represent contact with the bulk fluid:

$$N_B = k_c\left(C_B^{\text{bulk}} - C_B\right) \tag{8}$$

where C_B^{bulk} is equal zero.

Diffusion coefficients of Rhodamine B and BSA-FITC in hydrogel were evaluated by Fluorescence Recovery After Photobleaching method (FRAP) using Leica TCS SP5 microscope. The experiment was conducted in water at 20°C and the diffusion values obtained are in good agreement with those found in literature.[30,31]

RESULTS

Nanofibrous mats characterization

For the experimental verification we used two materials with different Rhodamine B dye concentration in nanofibers: 2.8% wt and 4.4% wt (Table I, materials M1, M2). We tested two different polymer materials with the same BSA-FITC dye concentration (2% wt) entrapped in water filled vesicles (Table I, materials M3, M4) [Figure 4(a,b)].

Nanofiber mats made by standard electrospinning method from PDLG polymer (M1, M2), formed densely packed randomly oriented fibrous material with wide distribution of fiber diameters (see Table I). For the same polymer used the emulsion electrospinning formed thick, straight nanofibers with narrow size distribution. In the material made by electrospinning from PLC polymer emulsion we observed mat structure of thin and wide nanofibers (wide size distribution).

The same materials M3 and M4 made of two polymers PDLG and PLC, containing BSA-FITC dye, were additionally examined with SEM after drug release experiment in PVA–borax hydrogel. The aim was to find an impact of alkaline hydrogel on nanofibers surface or morphology. Hence, after

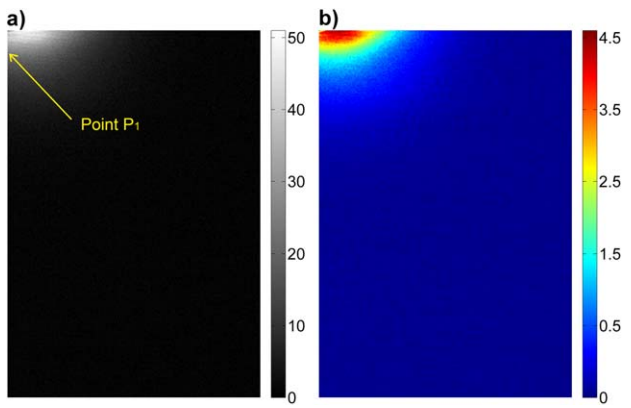

FIGURE 6. a) Rhodamine B intensity and b) calculated Rhodamine B concentration in the cuvette. Pictures present one half of the cuvette (left edge—axis of symmetry). [Color figure can be viewed in the online issue, which is available at wileyonlinelibrary.com.]

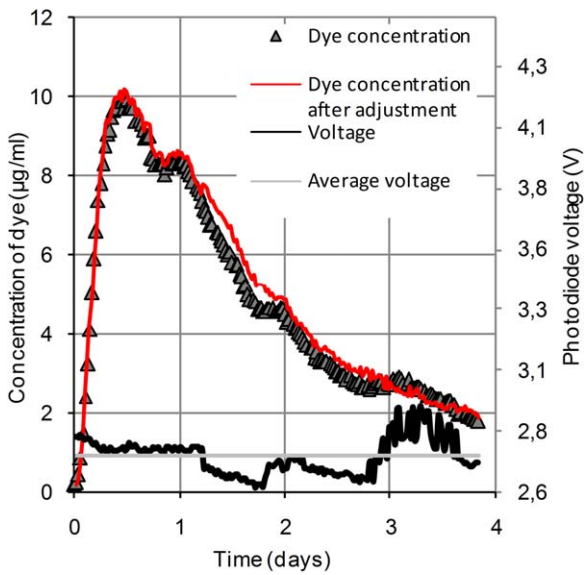

FIGURE 7. Concentration of Rhodamine B (gray triangles) in point P_1 and measured photodiode voltage corresponding to laser power (thick black line). Red line presents concentration adjusted to voltage fluctuations. Horizontal gray line represents average value of measured voltage. [Color figure can be viewed in the online issue, which is available at wileyonlinelibrary.com.]

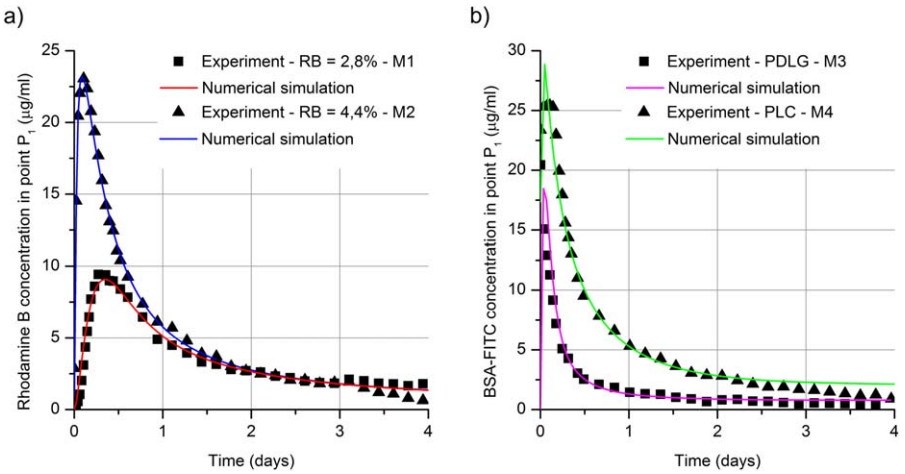

FIGURE 8. Real-time concentration profile of a) Rhodamine B, b) BSA-FITC in the point P_1 *vs.* time (only every tenth point presented for readability). Points represent experimental data. Lines represents results from numerical simulations with parameters of mathematical model k_{ads}, k_{des} fitted. [Color figure can be viewed in the online issue, which is available at wileyonlinelibrary.com.]

approximately 4 days of experiment, materials were washed with deionized water and left for drying. SEM micrographs shows no difference in nanofibers morphology and lack of any visible surface changes in case of PDLG polymer with dye [compare Figures 4(a) and 5(a)]. Small changes in PLC with dye nanofibers are noticeable [compare Figures 4(b) and 5(b)].

Drug transport in PVA hydrogel

We placed nanofibrous material on the PVA hydrogel and recorded distribution of fluorescence intensity of model drug using digital camera at the intervals of 5 min. Figure 6(a) presents an example image (material is not visible in the picture) taken at the time $t = 6$ h from the start of the experiment. Scale represents pixel values from 0 to 255. Figure 6(b) presents concentration field calculated from the image with use of the calibration curve.

We analyzed groups of images from single experiment to find real time concentration profile (Figure 7). Small fluctuations of light intensity, related to laser power variation can be observed (black solid line). For comparison, average output voltage from the photodiode (horizontal gray line) is presented. These fluctuations were used to normalize dye concentration profile. Raw data (gray triangles) of dye concentration in point P_1 were altered by multiplication of concentration value by coefficient dependent on the value of voltage. This process led to smoother concentration profile (red line).

Dyes concentration data measured (points) and fitted in numerical simulations (lines) for the point P_1 are presented in Figure 8(a) (Rhodamine B) and Figure 8(b) (BSA-FITC). For material with higher Rhodamine B content [4.4% wt; Figure 8(a) blue line], high concentration at the point P_1 was detected 3 h after the experiment started. For material with lower Rhodamine B concentration [2.8% wt; Figure 8(a) red

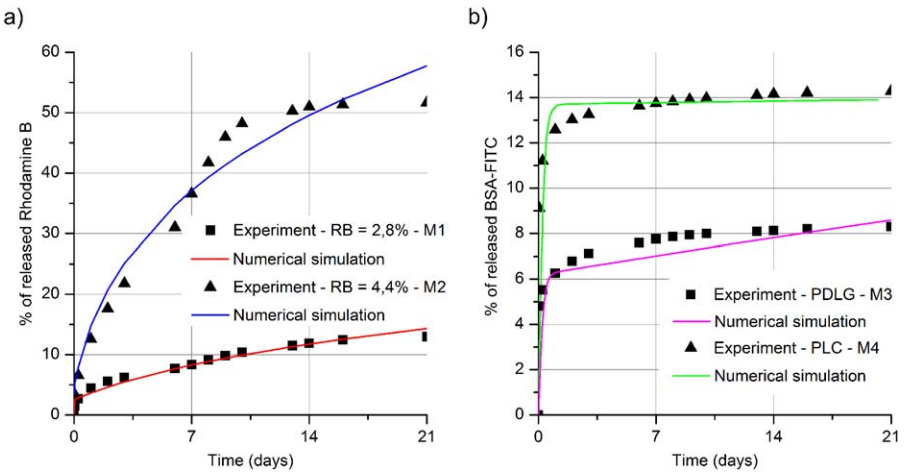

FIGURE 9. Release profile from materials with two different initial concentration for Rhodamine B a) BSA-FITC b). Drug release experiment was conducted with standard methods in vials filled with buffer. Points represent experimental data. Lines represent results from numerical simulations with parameters of mathematical model k_{ads}, k_{des} fitted. [Color figure can be viewed in the online issue, which is available at wileyonlinelibrary.com.]

line] the peak value was more than two times lower and observed 10 h after the experiment started. The 7 h shift in the peak value was probably due to smaller burst release in material with lower concentration of Rhodamine B.

Comparison of two materials made from different polymers showed maximum concentration approximately 2 h after drug release process started. Release of BSA-FITC from water vesicles near nanofibers surface facilitated transport of drug molecules to the surrounding hydrogel. Material made from PLC polymer [Figure 8(b) green line] released higher amount of dye, causing 1.5 times higher concentration peak in the hydrogel [compare Figure 9(b)]. Small changes in concentration profile in the point P_1 can be observed for PDLG polymer [Figure 8(b) magenta line] appearing as a very fast decrease of concentration after the peak.

Kinetic parameters calculated from experimental data of drug release in PVA hydrogel are presented in Table II.

Profile of drug release from material

Drug release is commonly determined at 37°C in PBS buffer. Cumulative dye released is referenced to total dye mass present in material and information about fraction of drug released to fluid is obtained. The cumulative mass of released Rhodamine B is presented in Figure 9(a). For 4.4% dye content small burst release is observed (blue line). After 3 weeks material released approximately 50% of dye present in nanofibers. Material of 2.8% released dye gradually. Only 15% of dye was released after 3 weeks (red line). Relatively high burst release was observed for materials made by electrospinning of emulsion. Material made of PLC polymer released dye rapidly, 13% of dye was liberated in 3 days, and reached release plateau at 14% of total drug content. Nanofibers made of PDLG released higher dose of dye in day 1 and slowly released dye reaching plateau at 8%. Almost two times higher value of released mass in case of PLC compared with PDLG polymer may be attributed to the presence of water vesicles closer to the surface of nanofibers. In both cases almost 90% of initial dye mass remained in nanofibrous structure and will be released during gradual degradation of polymers in time of months.

Kinetic parameters fitted from experimental data of drug release in PBS solution are presented in Table II.

Dye concentration value in function of distance from the material

Concentration values along line L_1 (Figure 3) for different times: 1, 6, 24, and 48 h were compared with values from numerical model. Results from numerical simulations used in this comparison were presented in drug transport in PVA hydrogel section, during the fitting of concentration profile for the point P_1 [Figure 8(a,b)].

For material M1 [Figure 10(a)] with lower dye concentration (2.8%) in PDLG, after 1 h of experiment Rhodamine B diffused into 1 mm depth of the hydrogel. At the beginning of the experiment, concentration near the material were five times smaller than after 6 h. The concentration profiles for experimental data and numerical fit are merely overlapping. For lower initial dye concentration in the material, burst release was smaller and resulted in lower dye concentration in hydrogel measured near the material surface.

In the case of material M2 [Figure 10(b)], with higher Rhodamine B content (4.4%) in PDLG, numerical simulations fit experimental data at 1, 24, and 48 h. For 6 h from the start of drug evaluation, numerical model suggests higher concentration at greater distance from the material. Also diffusion depth for this material was smaller than in material M1, suggesting that material showed burst release and later on gradually decrease dye release.

Material M3 [Figure 10(c)] made from PDLG polymer by electrospinning of emulsion with BSA-FITC showed small burst release to the hydrogel. Nearly no release of BSA-FITC was observed for longer time of experiment, while most of the drug was still present in the nanofibers. Overestimation of drug concentration in the numerical model was observed for short times from start of the experiment. Especialy for time equal 6 h, the experimental data showed two times smaller depth of dye diffusion comparing with the results from the numerical model.

Nanofibrous mat made of PLC polymer [material M4, Figure 10(d)] released high dose of dye resulting in the higher concentration near the material at the beginning of the experiment. In this case, results given by numerical simulations underestimated dye concentration values near the material and predicted deeper diffusion into the hydrogel. Numerical simulations for other experimental times relatively well reflect the results obtained during the experiment.

DISCUSSION

In recent years, interest in drug delivery systems based on nanofibers resulted in fabrication of materials with various drugs including: growth factors, anticancer agents or vitamins. Estimation of major release parameters is essential to build an optimal drug delivery system for various applications in tissue engineering and regenerative medicine. Several parameters like: polymer concentration in electrospinning solution, fibers diameter, fibers arrangement in material, drug initial concentration, type of polymer, electrospinning method can significantly affect desorption release process and subsequent transport of drug from the material.

Presented here PVA hydrogel system used for drug release evaluation together with laser light sheet method gave exact information about dye concentration in the surroundings of nanofibrous material. Our direct method of concentration determination if compared to method presented by Sindhwani et al. gives more accurate results.[14] It allows to avoid inaccurate evaluation of two-dimensional planar projection of three-dimensional object. Additionally, optical scanning of the whole PVA hydrogel (e.g. by rotation of the cuvette) may give us information about drug transport in all directions.

Comparing kinetic parameters obtained from numerical model for release in PBS solution and PVA hydrogel (Table II) one can see that for the same materials, obtained desorption constants are even two orders of magnitude higher in case of release in PVA hydrogel than in PBS solution, with relatively similar values of adsorption constants. Hence more dye (or

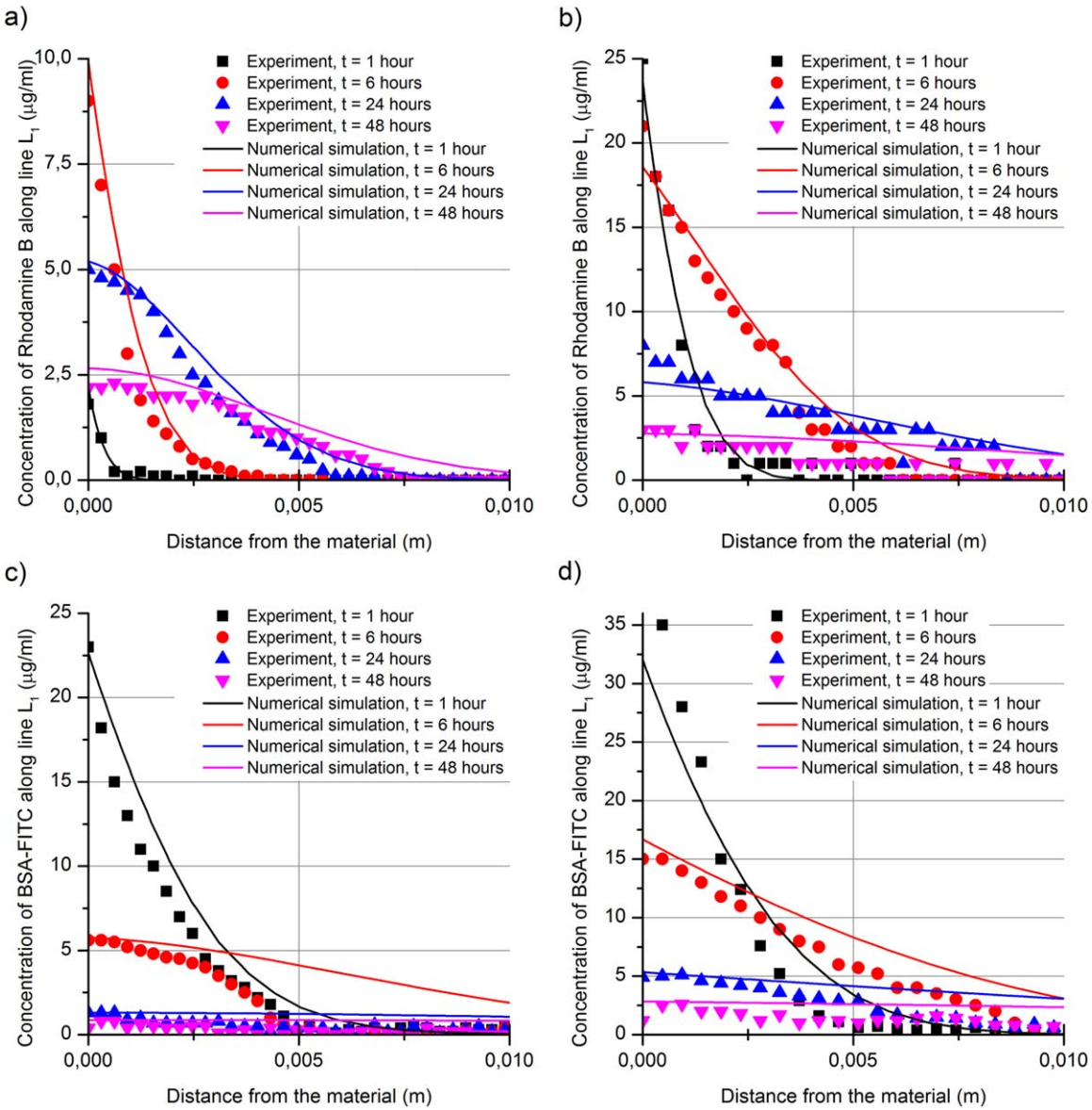

FIGURE 10. Dye concentration in hydrogel in the function of distance from the materials for different times of the experiment: 1 h, 6 h, 1 day, and 2 days. Materials containing Rhodamine B: a) M1, b) M2 and BSA-FITC: c) M3, d) M4. Points represent experimental data, lines represent numerical simulations. [Color figure can be viewed in the online issue, which is available at wileyonlinelibrary.com.]

drug) will be released in shorter time and subsequently diffusive mass transport is the most important. Increase of desorption constant in case of PVA hydrogel may be due alkaline properties of the hydrogel and reducing strength of dye—polymer interaction. For release in hydrogel, for material containing 2.8% wt of Rhodamine B desorption and adsorption were two and seventy times faster comparing to material with 4.4% wt of dye. Faster adsorption resulted in more than two times lower maximum concentration [Figure 8(a)]. Results for materials made of two different polymers show slightly faster desorption and slower adsorption of dye on PLC material. This effect can be associated with occurrence of dye filled vesicles close to the surface of fibers or higher surface to volume ratio related to smaller diameter of PLC fibers (Table I). To compare precisely difference in drug release from different polymers, process' parameters should be altered to obtain similar fiber distribution in both materials. Materials with Rhodamine B released in PBS solution (Table II) showed two times faster desorption from material with higher dye content. As in the case of release in the hydrogel, material made of PLC polymer released more BSA-FITC dye [Figure 9(b)] comparing to PDLG material. The low value of mass transfer coefficient calculated for release in PBS solution for materials M3 and M4 suggests that mass transfer across boundary Γ_1 and Γ_2 limits the drug release.

Numerical results can give us insight on concentration field obtained for different material parameters, like initial concentration, porosity or diameter of fibers in the material. Information about dye concentration at different distances from the material gives information about possibility to exceed toxic

concentration of drug, or values below minimal therapeutic concentration, and can be used for drugs applied *in vivo*. Data obtained with this method can be compared with literature reports for specific drugs, e.g. experiments performed *in vivo* with radiolabeled drugs on animal models.[32,33]

CONCLUSIONS

In this article we showed simple method to estimate local drug concentration field resulted from release of dye from nanofibrous mats. We proposed and investigated application of PVA-borax hydrogel to imitate biological tissue as brain model phantom. Fast preparation of the hydrogel and little light scattering make it very promising material for the use in study of drug delivery systems. Results from the numerical model showed good agreement with the experimental data. In the separate numerical study we show parametric analysis elucidating possibility to optimize structure of the nanofiber mat.

ACKNOWLEDGMENTS

The first author has been supported with a scholarship from the European Social Fund, Human Capital Operational Programme. The support of the National Centre for Research and Development Project is acknowledged. Grant nr: NR13008110.

REFERENCES

1. Fu SZ, Meng XH, Fan J, Yang LL, Wen QL, Ye SJ, Lin S, W BQ, Chen LL, Wu JB, Chen Y, Fan JM Li Z. Acceleration of dermal wound healing by using electrospun curcumin-loaded poly(ε-caprolactone)-poly(ethylene glycol)-poly(ϵ-caprolactone) fibrous mats. J Biomed Mater Res B Appl Biomater 2013;1–10.
2. Srouji S, Ben-David D, Lotan R, Livne E, Avrahami R, Zussman E. Slow-release human recombinant Bone morphogenic protein-2 embedded within electrospun scaffolds for regeneration of bone defect: In vitro and in vivo evaluation. Tissue Eng Part A 2011;17: 269–277.
3. Wang HB, Mullins ME, Cregg JM, Hurtado A, Oudega M, Trombley MT, Gilbert RJ. Creation of highly aligned electrospun poly-L-lactic acid fibers for nerve regeneration applications. J Neural Eng 2009;6:1–15.
4. Kijeńska E, Prabhakaran MP, Swieszkowski W, Kurzydlowski KJ, Ramakrishna S. Electrospun bio-composite P(LLA-CL)/collagen I/collagen III scaffolds for nerve tissue engineering. J Biomed Mater Res B Appl Biomater 2012;100:1093–1102.
5. Feng ZQ, Lu HJ, Leach MK, Huang NP, Wang YC, Liu CJ, Gu ZZ. The influence of type-I collagen-coated PLLA aligned nanofibers on growth of blood outgrowth endothelial cells. Biomed Mater 2010;5:1–8.
6. Ding S, Li J, Luo C, Li L, Yang G, Zhou S. Synergistic effect of released dexamethasone and surface nanoroughness on mesenchymal stem cell differentiation. Biomater Sci 2013;1:1091–1100.
7. Kidoaki S, Kwon IK, Matsuda T. Mesoscopic spatial designs of nano- and microfiber meshes for tissue-engineering matrix and scaffold based on newly devised multilayering and mixing electrospinning techniques. Biomaterials 2005;26:37–46.
8. Motealleh B, Zahedi P, Rezaeian I, Moghimi M, Abdolghaffari AH, Zarandi MA. Morphology, drug release, antibacterial, cell proliferation, and histology studies of chamomile-loaded wound dressing mats based on electrospun nanofibrous poly(ε-caprolactone)/polystyrene blends. J Biomed Mater Res B Appl Biomater 2013;100:1–11.
9. Wang Y, Wang B, Qiao W, Yin T. A novel controlled release drug delivery system for multiple drugs based on electrospun nanofibers containing nanoparticles. J Pharm Sci 2010;12:4805–4811.
10. Szentivanyi A, Chakradeo T, Zernetsch H, Glasmacher B. Electrospun cellular microenvironments: Understanding controlled release and scaffold structure. Adv Drug Deliv Rev 2011;63:209–220.
11. Peng H, Zhou S, Guo T, Li Y, Li X, Wang J, Weng J. In vitro degradation and release profiles for electrospun polymeric fibers containing paracetanol. Colloids Surf B Biointerfaces 2008;66:206–212.
12. Stylianopoulos T, Diop-Frimpong B, Munn LL, Jain RK. Diffusion anisotropy in collagen gels and tumors: The effect of fiber network orientation. Biophys J 2010;99:3119–3128.
13. Gandhi M, Srikar R, Yarin AL, Megaridis CM, Gemeinhart RA. Mechanistic examination of protein release from polymer nanofibers. Mol Pharm 2009;6:641–647.
14. Sindhwani N, Ivanchenko O, Lueshen E, Prem K, Linninger A. Methods for determining agent concentration profiles in agarose gel during convection-enhanced delivery. IEEE Trans Biomed Eng 2011;58:626–632.
15. Chen ZJ, Broaddus WC, Viswanathan RR, Raghavan R, Gillies GT. Intraparenchymal drug delivery via positive-pressure infusion: Experimental and modeling studies of poroelasticity in brain phantom gels. IEEE Trans Biomed Eng 2002;49:85–96.
16. O'Brien CC, Finch CH, Martens P, Barber TJ, Simmons A. Development of an in vitro method for modeling drug release and subsequent tissue drug uptake and deposition in a pulsatile flow network. Conf Proc IEEE Eng Med Biol Soc 2011;3262–3265.
17. Błoński S, Domagalski P, Dziubiński M, Kowalewski TA. Hydrodynamically modified seeding for micro-PIV. Arch Mech 2011;63: 163–182.
18. Kowalczyk T, Nowicka A, Elbaum D, Kowalewski TA. Electrospinning of bovine serum albumin. Optimization and the use for production of biosensors. Biomacromolecules 2008;9:2087–2090.
19. Andrychowski J, Frontczak-Baniewicz M, Sulejczak D, Kowalczyk T, Chmielewski T, Czarnicki Z, Kowalewski TA. Nanofiber nets in prevention of cicatrisation in spinal procedures. Experimental study. Folia Neuropathol 2013;51:147–157.
20. Sulejczak D, Andrychowski J, Kowalczyk T, Nakielski P, Frontczak-Baniewicz M, Kowalewski TA. Electrospun nanofiber mat as a protector against the consequences of brain injury. Folia Neuropathol 2014;52:56–69.
21. Lee JB, Yang DH. Highly porous electrospun nanofibers enhanced by ultrasonication for improved cellular infiltration. Tissue Eng Part A 2011;17:2695–2702.
22. MATLAB Release 2012b, The MathWorks, Inc., Natic, Massachusetts, United States.
23. Zhou Y, Wu XY. Finite element analysis of diffusional drug release from complex matrix systems. I. Complex geometries and composite structures J Controlled Release 1997;49: 277–288.
24. Galdi I, Lamberti G. Drug release from matrix systems: Analysis by finite element methods. Heat Mass Transf 2011;48:519–528.
25. Tzafriri AR. Mathematical modeling of diffusion-mediated release from bulk degrading matrices. J Controlled Release 2000;63:69–79.
26. COMSOL Release 4.3a, COMSOL, Inc., Burlington, Massachusetts, United States.
27. Nakielski P, Kowalczyk T, Kowalewski TA. Modeling drug release from materials based on electrospun nanofibers. In: Proceeding of the COMSOL Conference October 23-25, 2013, Rotterdam. Available at: http://www.comsol.com/paper/download/181521/nakielski_paper.pdf.
28. Clague DS, Phillips RJ. Hindered diffusion of spherical macromolecules through dilute fibrous media. Phys Fluids 1996;7:1720–1730.
29. Amsden B, Solute diffusion within hydrogels. Mechanisms and models. Macromolecules 1998;31:8382–8395.
30. Gendron PO, Avaltroni F, Wilkinson KJ. Diffusion coefficients of several rhodamine derivatives as determined by pulsed field gradient-nuclear magnetic resonance and fluorescence correlation spectroscopy. J Fluoresc 2008;18:1093–1101.
31. Shkilnyy A, Proulx P, Sharp J, Lepage M, Vermette P. Diffusion of rhodamine B and bovine serum albumin in fibrin gels seeded with primary endothelial cells. Colloids Surf B Biointerfaces 2013; 93:202–207.
32. Krewson CE, Saltzman WM. Transport and elimination of recombinant human NGF during long-term delivery to the brain. Brain Res 1996;727:169–181.
33. Krewson CE, Klarman ML, Saltzman WM. Distribution of nerve growth factor following direct delivery to brain interstitium. Brain Res 1995;680:196–206.